Southern Hemisphere Synoptic Weather from a Satellite Scatterometer

GAD LEVY

Department of Atmospheric Sciences, Oregon State University, Corvallis, Oregon

ROBERT A. BROWN

Department of Atmospheric Sciences, The University of Washington, Seattle, Washington

(Manuscript received 2 July 1990, in final form 8 May 1991)

ABSTRACT

Analyses of remotely sensed wind vector data from six satellite passes over parts of the Southern Ocean during September 1978 are shown. Winds are input to a planetary boundary layer model to produce sea level pressure fields. These are compared to the Australian Bureau of Meteorology conventional mean sea level pressure and to the European Centre for Medium Range Weather Forecasts pressure analyses. The analyses suggest that the Southern Hemisphere synoptic-scale pressure gradients for the cases studied are significantly stronger than those analyzed by the weather services. Compared to the Northern Hemisphere, serious deficiencies in all analysis schemes are revealed. However, it appears that remotely sensed data added to standard analysis techniques and satellite imagery can greatly enhance analysis and prognosis in remote oceanic regions and improve climatological flux estimates in the Southern Hemisphere.

1. Introduction

The lack of adequate data has long been a major obstacle to progress in atmospheric and oceanographic research and operations on all scales. This is especially true for synoptic and subsynoptic analyses and prognoses in oceanic regions such as the Southern Ocean. As a result, the few meteorological studies conducted in the Southern Hemisphere (SH) have focused on general circulation aspects where the lack of detailed information, although still a serious impediment, is not as crucial for the analysis. More detailed studies were made in specific years of the International Geophysical Year (IGY, 1957–58) and the First GARP Global Experiment (FGGE) year (1979). These studies (van Loon 1972, 1980; Trenberth 1979, 1981, 1982; Physick 1981) revealed that the high-frequency transients (i.e., synoptic-scale storms) dominate the eddy transports, more so than their Northern Hemispheric (NH) counterparts. They also indicated that there are regions of preferred cyclogenesis, with storms generally analyzed to be stronger over the South Atlantic and Indian oceans.

The additional buoy data from the FGGE year (1979) significantly improved the quality of the Australian Bureau of Meteorology (ABM) surface analyses and prognoses as discussed by Guymer and Le Marshall (1980). They showed significant differences from previous years, with great increase in the intensities of higher-latitude depressions. The magnitude of the differences in the operational products indicated that despite the anomalous global pressure pattern that year (Trenberth and van Loon 1981; Trenberth 1984), the changes in the analyses must be partially attributable to the incorporation of the buoy pressure observations. Since 1985 additional buoy data in the Southern Ocean are available to analyses as part of the Tropical Ocean Global Atmosphere (TOGA) Experiment. However, the vast ocean areas of the SH and the expense of operating an in situ dense observational network in the Southern Ocean make it impractical to collect buoy observations at the density and quality of the FGGE data over an extended period of time.

It seems plausible that significant improvement to analyses and forecasting of the SH could result from the incorporation of microwave remote sensor data. Experiments with the incorporation of scatterometer wind data in the European Centre for Medium Range Weather Forecasts (ECMWF) forecasting model have shown great potential for improved forecasting skills in the SH, although they have exposed some serious problems in data assimilation procedures (Anderson et al. 1987). Microwave remote sensor data would supplement the existing observational network with additional data at a density usable for routine synoptic-scale analyses. The primary goal of this study is to test an existing method of integrating scatterometer wind

Corresponding author address: Dr. Gad Levy, Dept. of Atmospheric Sciences, Oregon State University, Corvallis, OR 97331-2209.

data to provide surface-pressure analyses in the SH. The results are compared to standard operational analysis products for two case studies.

For storm-scale analysis, the Scanning Multichannel Microwave Radiometer (SMMR) and the *Seasat-A* Satellite Scatterometer (SASS) have been successfully combined to enhance midlatitude storm analyses (including one SH storm) by McMurdie et al. (1987). SASS-derived winds have been input to a planetary boundary layer (PBL) model to construct surface-pressure fields by Brown and Levy (1986). These fields were found to agree within 1–2 mb with the National Meteorological Center (NMC) analyses in the NH. In addition, the comparisons also revealed some subsynoptic-scale variability that was not shown in the NMC analyses.

There may be some fundamental differences in the dominant synoptic and mesoscale processes between the SH and the NH. Kidson (1988) found large low-frequency variations in the SH circulations, and van Loon (1980) concluded that in the SH the effect of the steady eddies on the transport of heat and momentum can be disregarded compared to that of the transient eddies. If this is indeed the case, the details of the storm-scale dynamics in the SH may be even more crucial for the understanding of the general circulation than in the NH. James and Anderson (1984) predict that a localized maximum of baroclinic activity will set up a large-scale circulation, which will tend to reinforce the local baroclinity (Hoskins et al. 1983). The relationship between thermal advection, stratification, the deformation field, and their effects on the PBL ageostrophic flow has been studied by Levy and Bretherton (1987), Levy (1989), and Levy and Tiu (1990). Hoskins (as reported by James and Anderson) pointed out that the streamlines resulting from the storm forcing along the SH storm track have a deformation field that will tend to increase the baroclinity at the start of the storm track and reduce it toward the end. Using the high-resolution SASS winds, a better estimate of this deformation field may be possible.

Australian operational analyses in the SH prior to 1979 relied heavily on deviations from climatology inferred from satellite images and case studies (Le Marshall et al. 1985). Manual methods were used to specify mean sea level pressure and the 1000–500-mb thickness from satellite cloud imagery where no other data were available. In this paper, we show two synoptic cases from 1978 where both the ABM operational and a subsequent ECMWF data assimilation–model analysis are compared to surface-pressure analysis based solely on scatterometer data. In the next two sections we describe the instrument, the data, the PBL model, and the analysis methods used. Section 4 compares and contrasts the different analyses. Finally, in section 5 we discuss the consequences of our results to basic science and operational questions.

2. Instrument and data

The analyses in this paper are based on scatterometer-retrieved (SASS) data. The SASS radar emits electromagnetic radiation at 14.6 GHz, which is Bragg-scattered back by short gravity-capillary ocean waves. The strength of the return signal is related to the amplitude and density of these wind-generated waves. A model is used to infer the wind speed and wind direction from the backscatter signal (Brown et al. 1982; Jones et al. 1982). Several methods to choose the correct wind direction from up to four possibilities emerging from the SASS data have been discussed by several authors (Endlich et al. 1981; Hoffman 1982, 1984; Yu and McPherson 1984; Levy and Brown 1986). The SASS has been reported to retrieve winds over the ocean with an accuracy of approximately 1.3 m s^{-1} in wind speed and 20° in wind direction by Born et al. (1982) with 50-km × 50-km resolution. This accuracy is expected to deteriorate under some conditions due to directional and speed biases.

There has been speculation from the earliest observations that the SASS signal may become saturated at high wind speeds. Anderson et al. (1987) suggest the possibility that the current algorithm overestimates low wind speeds and underestimates high wind speeds. The possibility that white-water effects change the SASS wind algorithm at high speed is still open. In light of this uncertainty over the SASS accuracy, sensitivity tests to examine the influence of such systematic errors on the integrated pressure were conducted and are discussed later.

The Seasat scatterometer surveyed the oceans during the 96 days of its mission (7 July 1978–10 October 1978) and provided two parallel swaths of wind measurements at the ocean surface, each approximately 500 km wide and separated by a latitudinally dependent gap of up to 400 km at the equator. The limited coverage of a single scatterometer within synoptic times (3–6 h) poses a major difficulty in using the data for global synoptic analysis. In addition, the relatively short period of the Seasat mission severely limits the usefulness of the data for climate studies. Nonetheless, Levy and Brown (1986) have shown that regional synoptic analyses of areas of approximately 2000 km × 2000 km can be produced by combining two successive swaths 100 min apart.

Figure 1 shows an overlay of three successive orbits used for the analyses in this study (orbits 1078, 1079, and 1080 on 10 September 1978). The time span for these three orbits is approximately 3.5 h, and they cover approximately a quarter of the southern oceans. In the future, more than one scatterometer will be needed to combine the data in synoptic time for global coverage.

The primary source of conventional data for the cases studied was the ABM-produced mean sea level pressure (MSLP) maps. In 1978, these were produced

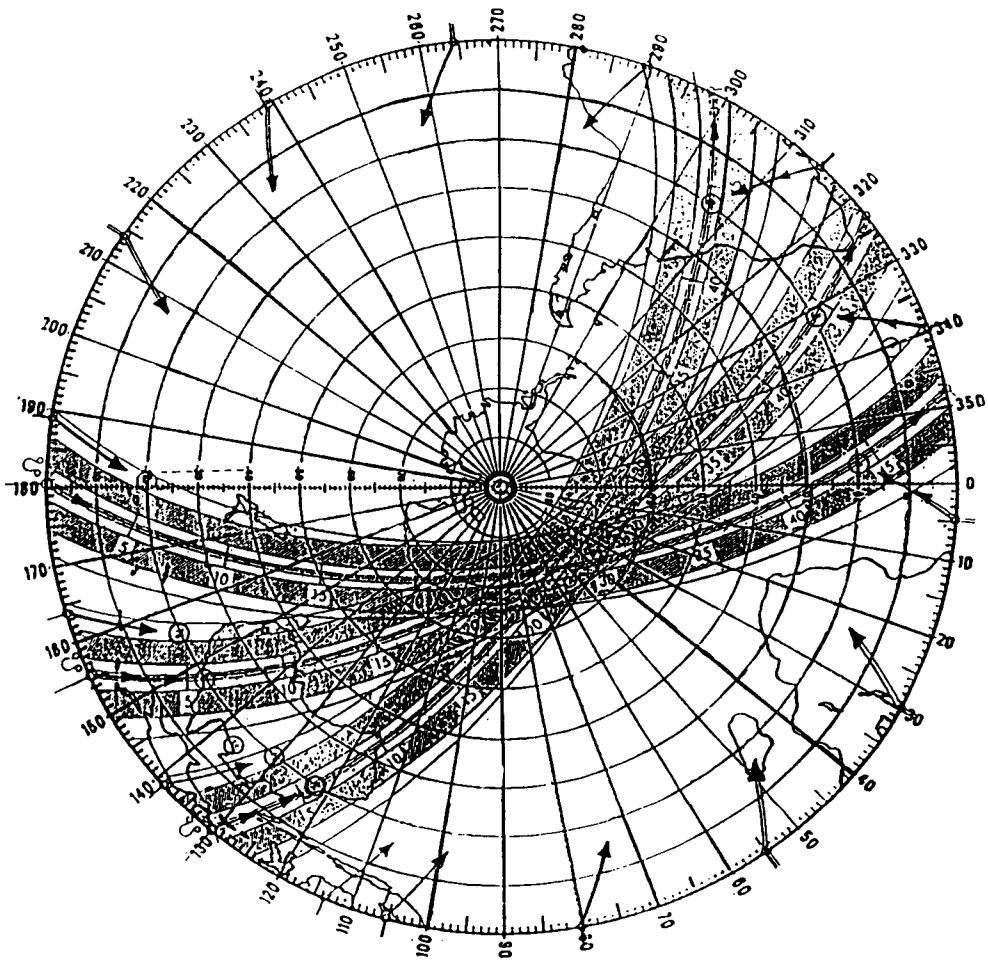

FIG. 1. An overlay of the three successive orbits used for the analyses in this study (orbits 1078, 1079, and 1080 on 10 September 1978).

manually, twice daily. In a few locations, reports of air temperature and dewpoint were included. In these maps, with the exception of a few ship and island reports, satellite imagery was the only data source in most of the SH oceans. Manual analysis of the cloud pictures provided patterns of 1000–500-mb thickness field and MSLP as deviations from climatology (Guymer 1978; Le Marshall et al. 1985). A small number of case studies was used to relate cloud patterns to observed deviation values. Large errors in the MSLP and in the location of surface fronts could be expected in all areas of no conventional data. The manual analyses were then used to provide first-guess fields for the analyses of temperature and geopotential height. In addition, numerical model 12-h forecast fields were included in the first-guess fields, and along with the observations, manual analyses were successively corrected to produce a gridded field in a data assimilation scheme. The manual analyses had a large impact on the final gridded analyses, however.

The PBL model can use air temperature and dewpoint reports to account for baroclinic and humidity effects in the boundary layer. When these data are available, cases that are run with and without these corrections in the model show the importance of these effects. A correction for the large-scale deformation field can be calculated based on SASS data alone. In the cases studied here, there was only one report of air–sea surface temperature difference (which was near-neutral stratification). Thus, the corrections for non-neutral PBL stratification were not applied.

3. Methods of analysis

This study concentrates on SH synoptic situations that were observed by the Seasat satellite around 1100

UTC 10 September 1978. The cases are grouped in two broad areas—one in the South Atlantic and the other in the Indian Ocean and south of Australia (see Figs. 1, 3, 4). These regions, and especially the belt between 30° and 60°S latitude, have been identified as areas where the storm tracks are located (Trenberth 1982). In this region, the sparsity of data had biased pre-FGGE analyses by showing spurious local variance maxima at locations of rawinsonde measurements (van Loon 1980). It is therefore interesting to use high-resolution data in these regions. We compare the MSLP produced with the ABM sea level pressure maps archived by the National Center for Atmospheric Research (NCAR) for 1100 UTC. The NCAR-archived maps are the gridpoint fields (47 × 47 polar stereographic grid mesh centered on the South Pole) produced by the ABM at the World Meteorological Centre (WMC) based on the hand analysis (Fig. 2) and the ABM assimilation procedure at the time (Le Marshall et al. 1985). In addition, the ABM analysis is compared to the 1200 UTC sea level pressure maps produced in 1986 as first-guess fields by the ECMWF four-dimensional (4D) data assimilation scheme described by Shaw et al. (1987). The latter analyses (dotted contours in Figs. 3a, 4a) are the results of the 6-h prediction of the ECMWF model (at a latitude–longitude grid resolution of approximately 1.12°). They weigh all the conventional observations but not the scatterometer observations.

Details on how the SASS data are handled are given in Levy and Brown (1986) and are briefly summarized here. SASS provides several possible directions at most points. The "correct" wind direction for the raw 50-km resolution SASS data is chosen by direct minimization to a first-guess field obtained from a 100-km resolution subjective analysis by the Jet Propulsion Laboratory (Wurtele et al. 1982; Baker et al. 1984). Since this procedure is prone to errors in the direction chosen, the SASS wind fields are rechecked for consistency with available surface-pressure charts and observations. This procedure of directional ambiguity removal and the associated potential error will be sim-

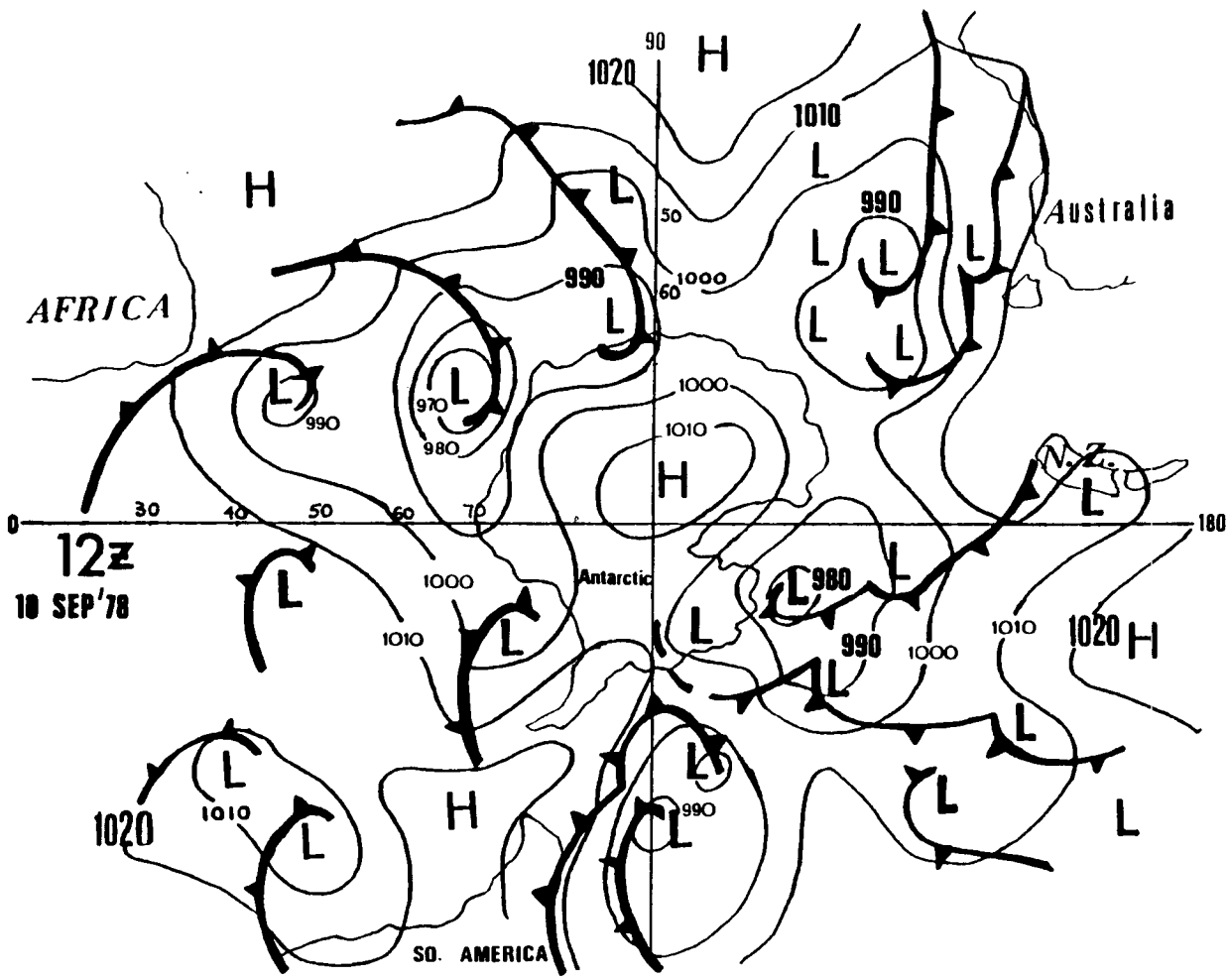

FIG. 2. The ABM manually produced SH surface analysis for 1200 UTC 10 September 1978.

plified considerably by the use of future scatterometers designed to eliminate the ambiguity.

The wind field is gridded on a 1° latitude–longitude grid mesh using a modified Cressman objective analysis scheme for each individual satellite pass. The gridded winds are used as a lower boundary condition to the PBL model. They are also used to calculate the divergence and deformation fields.

The PBL model used is a two-layer similarity model. In its basic form the model uses the Ekman–Taylor solution modified by the effects of finite perturbation large eddies as a solution to the steady-state momentum equations for the velocity profile throughout the Ekman layer (review by Brown 1982). The wind is assumed to be geostrophic at $z = h$, the top of the boundary layer, and has a finite value at the lower boundary (i.e., at the top of the surface layer). This solution is then matched with the solution for the logarithmic layer flow at the lower boundary, producing two stratification-dependent similarity equations that relate the surface wind to the geostrophic wind. Thus, by input of scatterometer winds, a field of geostrophic winds or pressure gradients can be obtained. These pressure gradients are assumed to be impressed on the surface or may be corrected for baroclinic effects through the PBL height, provided horizontal temperature gradients are available.

The observed wind in the PBL deviates from an idealized Ekman–Taylor profile due to several processes: 1) local horizontal inhomogeneities and varying horizontal gradients in the boundary layer, 2) nonlinear effects of organized large eddies in the PBL and, 3) baroclinic effects (i.e., vertical shear of the pressure gradients in the boundary layer).

In general, the solutions in both layers depend on stratification. In addition, the lower boundary conditions depend on the variable ocean surface roughness as a function of wind speed and stratification. The stratification-dependent, organized secondary circulations can transport considerable momentum vertically. This gives the entire PBL a fairly rapid response time to changes in surface conditions and thus justifies the implicit assumption of balance. The modified PBL solution that includes changes to the mean flow due to organized large eddies, stratification, and thermal wind effects is given in Brown and Levy (1986). The solution for the case of a horizontally inhomogeneous atmosphere is given in Levy (1989). Since SASS data provide the needed information for the horizontally inhomogeneous, neutrally stratified solution, this PBL solution is used to produce the pressure maps. The basic version is used for sensitivity tests and to isolate the effects of different correction terms. The agreement of even the basic model results with NMC analyses in strong cyclogenetic regions of the NH provides confidence in the procedure (Brown and Levy 1986).

Details of the surface-layer physics and parameterizations used in the model are given by Brown and Liu (1982). This kind of a diagnostic model is especially suitable for the treatment of horizontally dense datasets like that produced by the scatterometer. With an appropriate weight, such a diagnostic model can be incorporated into a complete data assimilation scheme where a prediction model and an initialization procedure would add dynamic constraints to the final first-guess (or analyzed) field (Hoffman and Louis 1990; Levy and Tiu 1990).

After the model is run producing a pressure-gradient field, a single pressure point can be used for the integration. Optionally, the procedure is started by optimizing the agreement between SASS analysis and a region of the ABM map, where there is confidence in the ABM analysis. We identify a region in each map where horizontal gradients in both the SASS and the ABM pressure fields are small and exhibit the same general features, where nearby pressure observations were available for the ABM analysis. The k gridded ABM pressure values within that region are then treated as "observations." The unknown constant of integration P_0 (assumed to be independent of x and y) can be estimated from the k observations by minimizing the sum of squares of the errors ϵ_k with respect to P_0. All of the gridded ABM pressure values are given equal weight in a least-squares estimate of P_0. The resulting SASS pressure fields are thus adjusted to match the ABM pressure fields in the chosen adjustment region. Though this procedure obviously produces SASS pressure fields that are liable to errors in the ABM analyses, the pressure-gradient information, which is really all that SASS alone can provide, is preserved. In recognition of the possibilities of errors in the actual pressure values, the following discussion focuses on gradients in the various pressure fields and the intensities and spatial scales of high and low pressure centers.

Each satellite pass is integrated separately. The composite regional maps are obtained by smoothing and averaging the individual passes (three for each synoptic map) to eliminate distortion due to propagation of systems within the time gaps between swaths, the accumulation of residual integration error, the lack of SASS observations over land, and the adjustment of each swath to a different limited region of the ABM map. Sensitivity tests are run to estimate the effects of stratification and baroclinity on the pressure fields.

4. Analysis

a. The hemispheric surface map

The ABM manually produced SH surface analysis for 1200 UTC 10 September 1978 is presented in Fig. 2. Most of the cyclonic systems in the synoptic map are associated with double lows and double fronts that are not resolved in the gridded ABM maps (Figs. 3a

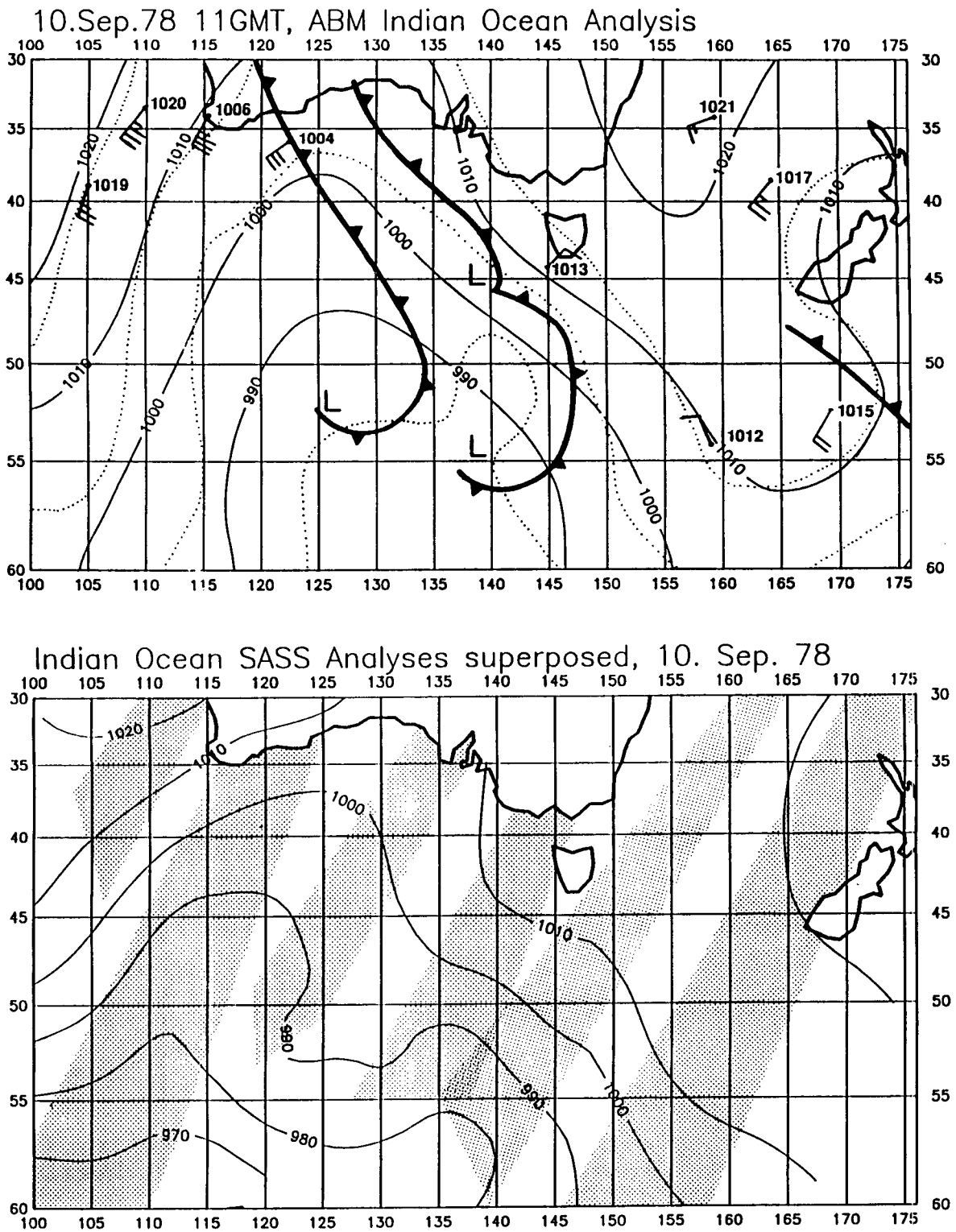

FIG. 3. (a) The ABM (1100 UTC) MSLP (solid) with the ECMWF (1200 UTC) MSLP (dotted), and all available island and ship sea level pressure and wind (using standard meteorological convention) observations and (b) the SASS–PBL model composite MSLP maps for the Indian Ocean region viewed by SASS revolutions 1078, 1079, and 1080 combined (0945–1300 UTC). Fronts in (a) are per ABM hand analysis for 1200 UTC, contour values for the ECMWF map are the same as for the nearest ABM contours. Areas scanned by SASS are stippled in (b).

and 4a, solid lines). Overall, in the belt between 30° and 60°S, there are 13 major frontal systems.

Two main midlatitude areas were scanned by the satellite within a 4-h time period (see Figs. 1, 3, and 4 for the individual passes within this period). One region covered is in the Indian Ocean and south of Australia extending from 100° to 176°E (Fig. 3, hereafter referred to as the Indian Ocean). The other region covered by the northward swath paths extends from 56°W to 42°E in the South Atlantic (Fig. 4). Seven out of the 13 baroclinic systems in Fig. 2 fall within these two regions.

b. *Indian Ocean storms*

Figure 3a shows the ABM (solid lines) and the ECMWF (dotted lines) pressure analyses and all the sea surface wind and pressure observations available for the ABM analysis for 1200 UTC 10 September 1978. With the exception of New Zealand's South Island, two island (Campbell and Macquarie islands) reports south of New Zealand and one report off the south Tasmanian coast, all of the surface observations and ship reports are limited to latitudes north of 45°S. There are no glaring inconsistencies between the pressure analyses and the pressure reports. Only the 1020-mb pressure report west of Australia (longitude 110°E) is slightly inconsistent with the analyses. The ABM analysis shows a large trough with two frontal systems directly south of Australia and another front south of New Zealand. The ECMWF (dotted lines) analysis does not show the 1020-mb contour that is supported by a 1021-mb observation over the Tasman Sea, but it shows a more distinct indication of the double low in the 990-mb contour. With the exception of the above mentioned 1020-mb contour, the agreement between the ABM and ECMWF analyses is better in the northern and eastern parts of the domain where more conventional observations exist. Some of the differences in these areas and the clearer indication of the double low can be the result of the finer ECMWF resolution. In the southwest, the ABM and ECMWF 990-, 1000-, and 1010-mb contours are over 500 km apart.

The SASS analysis is shown in Fig. 3b. The PBL baroclinic correction to the PBL model was based on four island reports (Amsterdam and McDonald, approximately 20° to the west of the region seen, and Campbell and Macquarie in the New Zealand sector). Despite substantial differences in details, the agreement in pattern and in location between the different analyses is good in the northern and eastern regions. Away from land, the SASS analysis essentially agrees with the basic frontal pattern, showing additional details. The trough in Fig. 3b has a short wave that is associated with the split multiple-low picture in the ECMWF (Fig. 3a) and the ABM hand-drawn (Fig. 2) analyses. When large-scale curvature effects were excluded from the PBL model, an even tighter pressure gradient formed in this region.

The main difference between the conventional analyses (Fig. 3a) and the SASS analysis is in the sharpness of the pressure gradients; the SASS field has a much deeper (by 20 mb) low in the southernmost sector that extends as far as 10°–15° to the west of the center of the ABM system. This westward extension results in a more zonal flow in this satellite analysis as compared to the mainly southerly flow in the southwest corner of the ABM analysis. Using a simple neutral drag-coefficient parameterization for momentum flux calculations, such a difference in pressure gradients may change the momentum flux estimates in this region by over 150%.

The possible reasons for the important differences between the analyses fall into the following categories: data availability to each analysis scheme, analysis resolution, and biases due to deficiencies in the different analysis procedures. The available ship and island pressure and wind reports are plotted in Fig. 3a. With the exception of one pressure observation discussed above and one coastal wind report in southwest Australia, they are in fair agreement with all three analyses. Resolution restrictions can explain the differences in the details between the SASS and ECMWF analyses (interpolated to a similar resolution) and between these and the coarser resolution ABM analysis, but not the differences in the intensity of the storm. The biases due to the deficiencies in the different analysis schemes and their possible effects on the analyses are discussed in section 5.

c. *South Atlantic storms*

Over the Atlantic, the ABM analysis (solid lines) shown in Fig. 4a has three separate low systems—a double low in the northwest, a weak front in the center, and a strong frontal band in the east. The corresponding ECMWF analysis (dotted lines) shows a deeper (by 10 mb) western cyclone and a very different structure of the eastern cyclonic system even south of South Africa, where observations were available to both analyses. In the SASS analysis shown in Fig. 4b, the western low pressure system is considerably deeper (20 mb deeper than ABM, 10 mb deeper than ECMWF) and has a different configuration, which is more indicative of a double-low structure (see also Fig. 2). Figure 4a also displays all of the island reports (an additional report in the Falklands to the west was available for the analyses). Unfortunately, with no ship reports in the area of largest differences, the observations are of little help in determining which analysis is correct.

The main disagreement among the different analyses in the double-front system in the northwestern part of the domain concerns the intensity of the storm. The fact that the ECMWF and the SASS pressure patterns

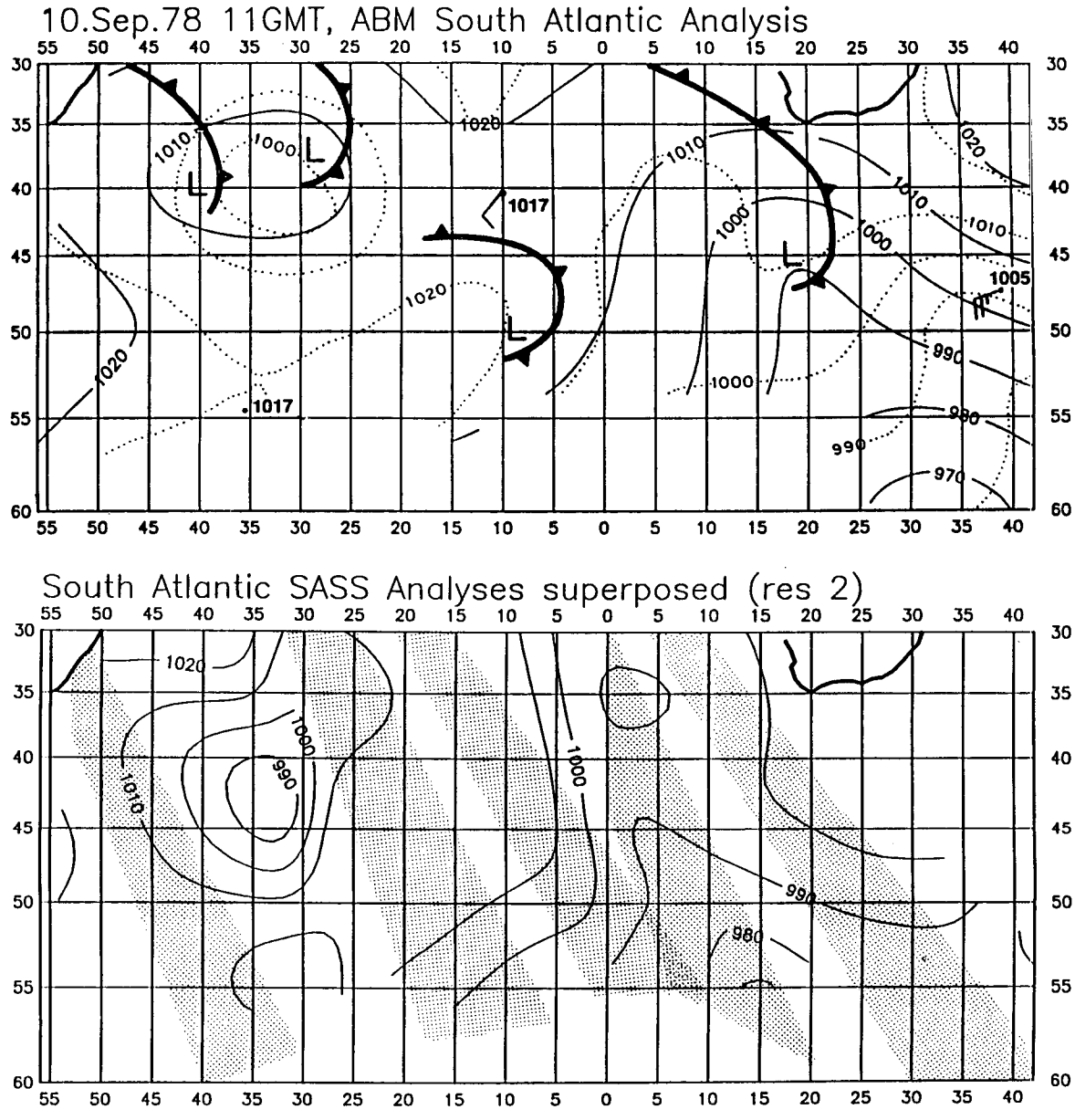

FIG. 4. As in Fig. 3, except for the South Atlantic.

(Fig. 4b) show considerably stronger gradients around the cyclone seems to support the conclusion that the ABM analysis underestimates the intensity of this storm. In an assimilation experiment conducted at the ECMWF (Anderson et al. 1987), the inclusion of SASS observations resulted in a difference of 75 m at the 1000-mb map in this area (approximately 10 mb). Thus, it is believed that the even stronger gradients seen in the SASS analysis of Fig. 4b reflect the true nature of the low-level circulation. Of some concern is the fact that the depression's center occurs at an area of a gap in the scatterometer data. However, it must be remembered that we are interpolating wind vectors so that such a result is not unusual (Brown and Levy 1986; Levy and Brown 1986). The baroclinity input to the model was based on observations on the Falkland and Gough islands. When baroclinic effects were excluded altogether, the pressure gradients were reduced but not enough to eliminate a 10-mb contour within the area shown in Fig. 4.

Farther to the east, the SASS (Fig. 4b) and the ECMWF (Fig. 4a, dotted lines) maps agree poorly with the ABM analysis and with each other, and it is impossible to determine which of the three is more cred-

ible (a single observation near 47°S, 38°W is consistent with the ABM rather than the ECMWF analysis). The effect of the large-scale curvature correction on the pressure in this region of cyclogenesis was to produce a westward extension of the system and an estimated lower central pressure.

5. Discussion and summary

We have used the high-resolution scatterometer data to look at six synoptic pressure fields in two broad ocean regions of the SH in spring. In the cases studied, we see strong surface winds in the SH associated with deep pressure systems with multiple frontal systems in agreement with the ABM hand analysis. However, we see systems that are 10–20 mb deeper than the ABM or the subsequent ECMWF analyses (which by themselves are deeper than their NH counterparts). In the South Atlantic, we also see large differences in the position of the storm centers.

Although we have presented just two synoptic case studies, and the analysis method has some serious limitations, there are several reasons to believe that the SASS-derived pressure gradients are representative of SH synoptic and mesoscale dynamics. First, we have performed similar analyses in NH areas in periods where major experiments took place (Brown and Levy 1986) and found remarkable agreement with the National Meteorological Center (NMC) pressure fields in the North Atlantic and the North Pacific. The NMC analyses are in general agreement with those of the ECMWF (Trenberth and Olson 1988). In the SH, the pressure gradient fields of the SASS, ECMWF, and ABM analyses agree fairly well in the northern sectors. However, farther south, the departure among the analyses grows rapidly. This is likely due to the ABM and ECMWF lack of data in the region away from continents and to the consistently dense input (even denser data) farther south of the SASS analysis.

Second, the ECMWF reanalysis performed in 1986 as part of assimilation experiments falls in between the ABM and the SASS analyses, but also tends to be conservative. The ECMWF analyses included many improvements that were not included in the ABM analysis performed in 1978. Nonetheless, data available for the ECMWF analyses were similar to those used by the ABM, and problems with proper assimilation of surface-pressure observations in the ECMWF scheme resulted in underestimation of the strength of depressions even during the FGGE enhanced observation period (Shaw et al. 1987; Trenberth and Olson 1988). Although the assimilation of SASS data in the ECMWF analysis (Anderson et al. 1987) encountered serious problems, the results of these experiments are in general agreement with our results.

Third, we have examined six cases (two parts of orbits 1078, 1079, and 1080) plus three other orbits not shown or discussed here (orbits 1068, 1073, and 1077) and found all of them to show similar characteristics. This consistency is obtained despite the lack of corrections to the PBL model due to stratification. Following the Seasat mission, starting in December 1978, the special FGGE drifting buoys network was installed. As a result, many additional surface-pressure observations from the drifting buoys became available to the ABM and were incorporated into their FGGE year (1979) analyses. These FGGE analyses are in general agreement with our (pre-FGGE) SASS analyses; the centers of SH FGGE period depressions are often analyzed as being approximately 20 mb deeper than would have been estimated based on the pre-FGGE conventional data, and much stronger westerly flow is regularly revealed south of Australia (Guymer and Le Marshall 1980).

There have been suggestions (Brown 1986; Anderson et al. 1987) that the SASS-1 algorithm underestimates wind speeds at the high wind-speed regime. Our analysis corrected wind speeds for the bias reported in Wentz et al. (1984). If instead there is a wind-speed–dependent bias, then the pressure gradients in our analysis would be biased low. We have conducted sensitivity tests and examined the influence of increasing the wind speed (by 1 m s^{-1}) on the pressure maps. At the 10-mb resolution, this effect could not be detected on the pressure maps. Similar sensitivity tests were conducted to estimate the potential effects that baroclinity and stratification have on the pressure fields. At a given stratification, the effect of the input horizontal temperature gradients resulted in ±0–4-mb difference. Similar differences resulted from stratification changes from unstable to stable regimes. If these effects are linearly combined, it is possible that differences of up to ±10 mb in extreme cases (e.g., sharp fronts with adjacent stable and unstable PBLs) could result. Since the relationship between these effects is not linear we expect the actual corrections to be lower in most cases.

The agreement among all three analyses is generally better in the Indian Ocean and close to the Australian continent where ABM analysis skills are better and data are more available. The pressure gradients diagnosed in this study suggest storms of similar intensity in both oceans. The South Atlantic systems exhibit the appearance of developing baroclinic eddies, while the Indian Ocean storms are larger in extent and have the appearance of mature and decaying baroclinic waves. One unique feature of the scatterometer data and of our PBL model is the ability to observe and account for the horizontal inhomogeneity (large-scale deformation field) and its effect on the PBL baroclinic structure. The results indicate that forcing by the large-scale flow generally tends to increase pressure gradients in the South Atlantic and decrease them in the Indian Ocean, where storms reach their mature and decaying stages.

Great improvements in analyses resulted from the additional surface-buoy information during the FGGE (and later the TOGA) periods. However, even with the improvements and changes in the ECMWF and ABM assimilation and analysis methods, problems with the proper assimilation of surface information over the SH oceans remain. By using only scatterometer data and by considering only the PBL model, we have avoided some of the assimilation problems and have exposed some problems with our method. Problems with directional ambiguity removal of SASS data and with the evaluation and incorporation of ageostrophic motions and thermal information in our method still exist. It is clear that SASS data alone are not sufficient for a complete surface analysis. However, it is evident that a satellite scatterometer (and other remotely sensed data) added to the cloud pictures and integrated into dynamical forecasting and diagnostic PBL models could allow the SH analysis to be improved to a quality comparable to that of the NH. We suspect that the stratification information may be more crucial for a forecasting model than it is for a diagnostic PBL model, since it may change the rate of baroclinic growth and increase the error with each time step. Techniques for data assimilation and for bridging over spatial and temporal gaps in data need to be developed before such data could be used routinely.

The higher winds, deeper lows, and more frequent small-scale variations seen by scatterometer will have many effects on flux calculations. The common bulk flux parameterizations depend on the near-surface wind (or geostrophic) speed. One can expect the estimates of the mean vertical fluxes of heat, moisture, momentum, and CO_2, based on these stronger winds, to be higher than previous calculations indicated. Meridional eddy transport by these systems may also be different. Long-term climatological estimates based on this information are also likely to change. Unfortunately, there have not been any new scatterometer data since the 1978 Seasat mission, and the value of reanalyzing the 3 months of the Seasat period with the scatterometer data is limited for climate diagnostics. We expect to apply this method of pressure-gradient analysis to the *ERS-1*, NSCAT, and EOS era scatterometers.

Acknowledgments. The authors would like to express their gratitude to the Australian Bureau of Meteorology, the European Centre for Medium Range Weather Forecasts, the Jet Propulsion Laboratory, and the National Center for Atmospheric Research (supported by the National Science Foundation) for providing the different datasets and analyses used in this study. The authors would also like to thank the National Aeronautics and Space Administration for providing support for this research under Grants NAS 5-30553, NAGW1770, and NSCAT/JPL at Oregon State University and the University of Washington. Comments by Steve Esbensen on an earlier version of this paper were helpful in improving this paper.

REFERENCES

Anderson, D., A. Hollingsworth, S. Uppala and P. Woiceshyn, 1987: A study of the feasibility of using sea and wind information from the ERS-1 satellite. Part 1: Wind Scatterometer Data. European Centre for Medium Range Weather Forecasts contract report 6297/86/HGE-I(SC), 121 pp. [European Centre for Medium Range Weather Forecasts, Shinfield Park, United Kingdom.]

Baker, W. E., R. Atlas, E. Kalnay, M. Halem, P. M. Woiceshyn, S. Peteherych and D. Edelmann, 1984: Large scale analysis and forecasting experiments with wind data from *Seasat-A* scatterometer. *J. Geophys. Res.*, **89,** 4927–4936.

Born, G. H., D. N. Held, D. B. Lame, R. G. Lipes, D. R. Montgomery, P. J. Rygh and J. F. Scott, 1982: Seasat data utilization project report. Rep. JPL D-36, 72 pp. Jet Propulsion Lab., Pasadena, CA.

Brown, R. A., 1982: On two layer models and the similarity functions for the PBL. *Bound.-Layer Meteor.*, **24,** 451–463.

——, 1986: On satellite scatterometer capabilities in air–sea interaction. *J. Geophys. Res.*, **91,** 2221–2232.

——, and W. T. Liu, 1982: An operational large-scale marine PBL model. *J. Appl. Meteor.*, **21,** 261–269.

——, and G. Levy, 1986: Ocean surface pressure fields from satellite-sensed winds. *Mon. Wea. Rev.*, **114,** 2197–2206.

——, V. J. Cardone, T. Guymer, J. Hawkins, J. E. Overland, W. J. Pierson, S. Peteherych, J. C. Wilkerson, P. M. Woiceshyn and M. Wurtele, 1982: Surface wind analysis for Seasat. *J. Geophys. Res.*, **87,** 3355–3364.

Endlich, R. M., D. E. Wolf, C. T. Carlson and J. W. Maresca, Jr., 1981: Oceanic wind and balanced pressure–height fields derived from satellite measurements. *Mon. Wea. Rev.*, **109,** 2009–2016.

Guymer, L. B., 1978: Operational application of satellite imagery to synoptic analysis in the Southern Hemisphere. Tech. Rep. 29, 50 pp. [Dept. of Science, Australian Bureau of Meteorology, Melbourne, Australia.]

——, and J. F. Le Marshall, 1980: Impact of FGGE data on Southern Hemisphere analyses. *Aust. Meteorol. Mag.*, **28,** 19–42.

Hoffman, R. N., 1982: SASS wind ambiguity removal by direct minimization. *Mon. Wea. Rev.*, **110,** 434–445.

——, 1984: SASS wind ambiguity removal by direct minimization. Part II. *Mon. Wea. Rev.*, **112,** 1829–1852.

——, and J. F. Louis, 1990: The influence of atmospheric stratification on scatterometer winds. *J. Geophys. Res.*, **95,** 9723–9730.

Hoskins, B. J., and N. V. West, 1979: Baroclinic waves and frontogenesis. Part II: Uniform potential vorticity jet flows—cold and warm front. *J. Atmos. Sci.*, **36,** 1663–1680.

——, I. N. James and G. H. White, 1983: The shape, propagation and mean flow interaction of large-scale weather systems. *J. Atmos. Sci.*, **40,** 1595–1612.

James, I. N., and D. L. T. Anderson, 1984: The seasonal mean flow and distribution of large scale weather systems in the Southern Hemisphere: The effects of moisture transports. *Quart. J. Roy. Meteor. Soc.*, **110,** 943–966.

Jones, W. L., L. C. Schroeder, D. H. Boggs, E. M. Bracalente, R. A. Brown, G. J. Dome, W. L. Pierson and F. J. Wentz, 1982: The *Seasat-A* satellite scatterometer: The geophysical evaluation of remotely sensed wind vectors over the ocean. *J. Geophys. Res.*, **87,** 3297–3317.

Kidson, J. W., 1988: Indices of the Southern Hemisphere zonal wind. *J. Climate,* **1,** 183–194.

Le Marshall, J. F., G. A. M. Kelly and D. J. Karoly, 1985: An atmospheric climatology of the Southern Hemisphere based on ten years of daily numerical analyses (1972–82): Overview. *Aust. Meteor. Mag.*, **33,** 65–85.

Levy, G., 1989: Surface dynamics of observed maritime fronts. *J. Atmos. Sci.*, **46,** 1219–1232.

——, and R. A. Brown, 1986: A simple objective analysis scheme for scatterometer data. *J. Geophys. Res.*, **91,** 5153–5158.

——, and C. S. Bretherton, 1987: On a theory of the evolution of surface cold fronts. *J. Atmos. Sci.*, **44,** 3413–3418.

——, and F. S. Tiu, 1990: Thermal advection and stratification effects on surface winds and the low-level meridional mass transport. *J. Geophys. Res.*, **95,** 20 247–20 257.

McMurdie, L. A., G. Levy and K. B. Katsaros, 1987: On the relationship between scatterometer derived convergences and atmospheric moisture. *Mon. Wea. Rev.*, **115,** 1281–1294.

Physick, W. L., 1981: Winter depression tracks and climatological jet streams in the Southern Hemisphere during the FGGE year. *Quart. J. Roy. Meteor. Soc.*, **107,** 883–898.

Shaw, D. B., P. Loenberg, A. Hollingsworth and P. Unden, 1987: The 1984/85 revisions of the ECMWF mass and wind analysis. *Quart. J. Roy. Meteor. Soc.*, **113,** 533–566.

Trenberth, K. E., 1979: Interannual variability of the 500 mb zonal mean flow in the Southern Hemisphere. *Mon. Wea. Rev.*, **107,** 1515–1524.

——, 1981: Observed Southern Hemisphere eddy statistics at 500 mb: Frequency and spatial dependence. *J. Atmos. Sci.*, **38,** 2585–2605.

——, 1984: Interannual variability of the Southern Hemisphere circulation: Representativeness of the year of the Global Weather Experiment. *Mon. Wea. Rev.*, **112,** 108–123.

——, and H. van Loon, 1981: Comments on "Impact of FGGE buoy data on Southern Hemisphere analyses." *Bull. Amer. Meteor. Soc.*, **62,** 1486–1489.

——, and J. G. Olson, 1988: An evaluation and intercomparison of global analyses from the National Meteorological Center and the European Centre for Medium Range Weather Forecasts. *Bull. Amer. Meteor. Soc.*, **69,** 1047–1057.

van Loon, H., 1972: Pressure in the Southern Hemisphere. *Meteorology in the Southern Hemisphere, Meteor. Monogr.*, No. 13, Amer. Meteor. Soc., 59–86.

——, 1980: Transfer of sensible heat in the atmosphere on the Southern Hemisphere: An appraisal of the data before and during FGGE. *Mon. Wea. Rev.*, **108,** 1774–1781.

Wentz, F. J., S. Peteherych and L. A. Thomas, 1984: A model function for ocean radar cross sections at 14.6 GHz. *J. Geophys. Res.*, **89,** 3689–3704.

Wurtele, M. G., P. M. Woiceshyn, S. Peteherych, M. Borowski and W. S. Appleby, 1982: Wind direction alias removal studies of Seasat scatterometer-derived wind fields. *J. Geophys. Res.*, **87,** 3365–3377.

Yu, T. W., and R. D. McPherson, 1984: Global data assimilation experiments with scatterometer winds from *Seasat-A. Mon. Wea. Rev.*, **112,** 368–376.